# Multi-Condition Conformal Selection

Qingyang Hao<sup>1</sup>, Wenbo Liao<sup>1,2</sup>, Bingyi Jing<sup>1</sup>, and Hongxin Wei<sup>1</sup>

<sup>1</sup>Southern University of Science and Technology <sup>2</sup>The Chinese University of Hong Kong

#### ABSTRACT

Selecting high-quality candidates from large-scale datasets is critically important in resource-constrained applications such as drug discovery, precision medicine, and the alignment of large language models. While conformal selection methods offer a rigorous solution with False Discovery Rate (FDR) control, their applicability is confined to single-threshold scenarios (i.e., y > c) and overlooks practical needs for multi-condition selection, such as conjunctive or disjunctive conditions. In this work, we propose the Multi-Condition Conformal Selection (MCCS) algorithm, which extends conformal selection to scenarios with multiple conditions. In particular, we introduce a novel nonconformity score with regional monotonicity for conjunctive conditions and a global Benjamini–Hochberg (BH) procedure for disjunctive conditions, thereby establishing finite-sample FDR control with theoretical guarantees. The integration of these components enables the proposed method to achieve rigorous FDR-controlled selection in various multi-condition environments. Extensive experiments validate the superiority of MCCS over baselines, its generalizability across diverse condition combinations, different real-world modalities, and multi-task scalability.

# 1 Introduction

In many practical scenarios with limited resources, it is essential to select a subset of candidates from a very large pool that best meet specific criteria for downstream processing. For instance, drug discovery screens compounds using properties like *logP* to avoid molecular docking pitfalls [1]; medical monitoring prioritizes high-risk patients via predictive systems [2]; and large language model (LLM) research employs selective procedures for output validation [3]. Across these domains, controlling the finite-sample *false discovery rate* (FDR) is crucial for conserving resources and mitigating risks. The reliance on machine learning model predictions, due to the frequent unavailability of true test responses, necessitates quantifying uncertainty for maintaining efficiency. *cfBH* [4] thus formulates the selection problem as a multiple hypothesis test by employing conformal *p*-values [5], which are constructed based on conformal prediction principles [6]. This multiple testing-based framework has been validated in areas such as LLM alignment [7] and extended in further studies such as *mCS* [8].

However, existing approaches restrict the hypothesis to a single condition of the form y>c, a formulation that is often insufficient in practical applications. In the concept of "drug-like" properties, compounds with medium logP are chosen by most practices [9], which exemplifies the need for conjunctive conditions (i.e.,  $c_1 < y < c_2$ ). Conversely, disjunctive conditions (i.e.,  $y < c_1$  or  $y > c_2$ ) are necessary in other contexts, such as early-warning systems that must activate when a target value exceeds or falls below critical thresholds [10, 11]. These instances highlight the necessity of selection under multi-condition settings.

In this paper, we extend the conformal selection framework to multi-condition settings, with a central goal of achieving finite-sample FDR control under both conjunctive and disjunctive conditions. We first show that naive combinations via intersection or union of single-condition selection results fail to preserve FDR control for multi-condition selection. To address this, we introduce a novel method *MCCS* equipped with rigorous theoretical guarantees. For conjunctive conditions, we design a tailored nonconformity function that targets intervals defined by simultaneous constraints; for disjunctive conditions, we introduce a global ranking mechanism over conformal *p*-values from individual conditions, followed by application of the Benjamini–Hochberg (BH) procedure [12].

The approach naturally generalizes to compound multi-interval targets and multivariate response settings, while maintaining finite-sample FDR guarantees.

Our method was rigorously evaluated on both simulated and real-world datasets. In simulations, it demonstrated superior performance over baseline methods, as evidenced by a tighter alignment between the achieved *false discovery proportion* (FDP) and the nominal FDR. For instance, in the experiment of the univariate case under conjunctive conditions with a nominal FDR of 0.3, the FDP achieved by baselines exhibited significant deviations, either excessively high (0.3766) or too low (0.2013), while our approach achieved the closest approximation (0.2874) without exceeding the nominal level. Additionally, results on textual, visual, and multimodal tasks also validate the practicality of our method in real-world applications. The selection capability was further validated in multi-class scenarios, enabling reliable selection of individual, multiple, or similar classes.

# 2 Preliminary

**Problem Setup.** We let  $\mathbf{x} \in \mathbb{R}^p$  represent the p-dimensional features, which are accessible in the entire dataset, and let  $\mathbf{y} \in \mathbb{R}^1$  denote the responses  ${}^1$ . In this paper, we mainly focus on the regression setting, and our work can be generalized to multi-class tasks as presented in Appendix D. The entire dataset is divided into a training dataset  $\mathcal{D}_{\text{train}} = \{\mathbf{x}_i, \mathbf{y}_i\}_{i=1}^n$  and a test dataset  $\mathcal{D}_{\text{test}} = \{\mathbf{x}_{n+j}\}_{j=1}^m$ , where the corresponding test responses  $\{\mathbf{y}_{n+j}\}_{j=1}^m$  are unobserved. The additional assumption is that samples  $\{\mathbf{x}_i, \mathbf{y}_i\}_{i=1}^{n+m}$  in the dataset are drawn i.i.d. from an unknown distribution  $\mathcal{D}_{X \times Y}$ .

The selection problem can be formulated as follows: Given a union of intervals  $I_{Target}$ , which can be a union of multiple one-sided-unbounded or bounded open intervals  $I_k$ , our goal is to identify a subset  $S \subseteq \{1, \ldots, m\}$  from  $\mathcal{D}_{\text{test}}$  such that as many test observations  $j \in S$  satisfy  $\mathbf{y}_{n+j} \in I_{Target}$  as possible, while controlling the FDR [12] below a user-specified level q. The FDR is defined as the expectation of the FDP among all selected observations:

$$FDR = \mathbb{E}[FDP], \quad FDP = \frac{\sum_{j=1}^{m} \mathbf{1} \{ j \in \mathcal{S}, \mathbf{y}_{n+j} \notin I_{Target} \}}{1 \vee |\mathcal{S}|}.$$
 (1)

Since an excessively low FDR can be trivially achieved by selecting very few samples, it is also important to evaluate whether a method retains an adequate number of selections that truly meet the target criteria. This aspect is quantified by the metric power:

Power = 
$$\mathbb{E}\left[\frac{\sum_{j=1}^{m} \mathbf{1}\left\{j \in \mathcal{R}, \mathbf{y}_{n+j} \in I_{Target}\right\}}{1 \vee \sum_{j=1}^{m} \mathbf{1}\left\{\mathbf{y}_{n+j} \in I_{Target}\right\}}\right].$$
 (2)

Ideally, a practical approach should simultaneously achieve an FDP that closely approximates, yet does not exceed, the nominal FDR, while maintaining a relevant high power.

**Conformal Selection.** The *cfBH* framework [4], building upon conformal prediction principles [6], is designed to guarantee finite-sample false discovery rate (FDR) control in conformal selection under a single condition. It performs multiple hypothesis testing by selecting candidates whose values exceed a pre-specified threshold c. For each test sample, a hypothesis test is constructed with the following hypotheses:

$$H_{0j}: y_{n+j} \le c$$
 vs.  $H_{1j}: y_{n+j} > c$ .

Rejection of  $H_{0j}$  indicates that the j-th sample is selected, as it's considered satisfying the condition. With the hypothesis test, the CS framework ensures FDR control via two core steps as follows.

First, it employs a nonconformity score  $V(\mathbf{x},y)$  that satisfies appropriate monotonicity constraints to quantify how atypical a response is given the input. For a calibration sample with observed response, the score is computed as  $V_i = V(\mathbf{x}_i, y_i)$ ; for a test sample with unobserved response, the score is evaluated at a predefined threshold c, yielding  $\hat{V}_{n+j} = V(\mathbf{x}_{n+j}, c)$ . Then, the conformal p-value for each test sample is derived from the rank of its nonconformity score relative to the calibration set. Lower p-values provide stronger evidence for selection, corresponding to rejection of the null hypothesis  $H_{0j}$ . Second, the framework applies the Benjamini–Hochberg (BH) procedure [12, 13], a widely adopted method in multiple testing, to these conformal p-values for FDR control. The monotonicity property of the nonconformity score, combined with the BH procedure, jointly guarantees finite-sample FDR control. However, the cfBH framework and its existing derivatives are exclusively confined to single-condition selection, overlooking the complexities of multi-condition conformal selection. This gap will be elaborated upon in the subsequent section.

<sup>&</sup>lt;sup>1</sup>Later, we will extend the univariate responses to multivariate in Section 4.4.

# 3 Multi-Condition Conformal Selection

In this section, we introduce the task of Multi-Condition Conformal Selection with detailed formulations, and demonstrate why the *cfBH* procedures [4] cannot be directly extended to this setting via simple set operations such as intersection or union.

## 3.1 Conditions and Selection Target

Single-condition CS refers to the process of comparing the response value  $\mathbf{y}$  against a single threshold. In contrast, multi-condition CS involves evaluation against multiple thresholds to determine target satisfaction. The fundamental types of multi-condition CS are conjunctive and disjunctive conditions, with more complex structures emerging from their combinations. For conjunctive conditions, such as those requiring  $\mathbf{y}_{n+j} > c_{k_L}$  and  $\mathbf{y}_{n+j} < c_{k_R}$ , the null hypothesis is defined as  $H_{0j}^k : \mathbf{y}_{n+j} \in (c_{k_L}, c_{k_R})$ , with the corresponding alternative hypothesis  $H_{1j}^k : \mathbf{y}_{n+j} \notin (c_{k_L}, c_{k_R})$ . This approach ensures that any null hypothesis, whether constructed from a single condition or a conjunction, can be mapped to a target interval  $I_k$ . Consequently, for disjunctive conditions, the selection target is logically extended to the union of the intervals associated with each individual hypothesis. That is, the composite hypothesis formed by combining all conditions may be expressed as follows:

$$H_{0j}^{combine}: \mathbf{y}_{n+j} \in I_{Target}$$
 vs.  $H_{1j}^{combine}: \mathbf{y}_{n+j} \notin I_{Target}$ 

where  $I_{Target} = \bigcup_{k=1}^{K} I_k$ , each  $I_k$  denotes a one-sided-unbounded or bounded open interval. We present an intuitive illustration of multiple conditions in Figure 1.



Figure 1: Illustration of Single- and Multi-Condition.

### 3.2 conformal p-value

The conformal p-value serves as the critical link between the nonconformity score and the BH procedure. When the response  $\mathbf{y}_{n+j}$  is observable, we can compute the nonconformity score as  $V_i = V(\mathbf{x}_i, \mathbf{y}_i)$  for  $i = 1, \dots, n+m$ , where V is a nonconformity function based on  $\hat{\mu}$ , then the oracle conformal p-value would be defined as:

$$p_j^* = \frac{\sum_{i=1}^n \mathbf{1}\{V_i < V_{n+j}\} + U_j \left(1 + \sum_{i=1}^n \mathbf{1}\{V_i = V_{n+j}\}\right)}{n+1}$$
(3)

where  $U_i \sim \text{Unif}(0,1)$  is an independent random variable for tie-breaking.

To ensure finite-sample FDR control via the BH procedure, the conformal p-values must satisfy conservativeness  $(\mathbb{P}(p_j^* \leq \alpha) \leq \alpha)$  [5]. While this property holds for the oracle conformal p-value  $p_j^*$ , its computation is infeasible in practice since the test responses  $y_{n+j}$  are unobservable. Consequently, the nonconformity score  $V_{n+j} = V(\mathbf{x}_{n+j}, \mathbf{y}_{n+j})$  cannot be computed directly. Instead, we substitute it with  $\widehat{V}_{n+j} = V(\mathbf{x}_{n+j}, c_k)$ , where  $c_k$  denotes a prespecified threshold. This leads to the conformal p-value conformal p-value definition:

$$p_{j} = \frac{\sum_{i=1}^{n} \mathbf{1} \left\{ V_{i} < \widehat{V}_{n+j} \right\} + U_{j} \left( 1 + \sum_{i=1}^{n} \mathbf{1} \left\{ V_{i} = \widehat{V}_{n+j} \right\} \right)}{n+1}.$$
 (4)

To ensure the conservativeness of practical p-values  $p_j$ , the nonconformity score  $V(\mathbf{x}, \mathbf{y})$  must satisfy the following regional monotonicity:

**Definition 3.1** (Regional Monotonicity). ([8]) A nonconformity score  $V: \mathcal{X} \times \mathcal{Y} \to \mathbb{R}$  satisfies regional monotonicity if  $V(\mathbf{x}, \mathbf{y}') \leq V(\mathbf{x}, \mathbf{y})$  for all  $\mathbf{x} \in \mathcal{X}$ ,  $\mathbf{y}' \in R^c$ , and  $y \in R$ , where R represents the target region.

As shown in mCS [8], the practical p-values  $p_j$ , derived from a nonconformity measure satisfying regional monotonicity, are conservative and thus ensure FDR control. Note that the conservativeness of  $p_j$  here is not the usual statistical conservatism, but refers specifically to the following under  $H_0$ :  $\mathbb{P}(p_j \leq \alpha \text{ and } j \in \mathcal{H}_0) \leq \alpha, \forall \alpha \in (0,1)$ . This property nonetheless suffices to guarantee FDR control [8]. The key challenge is thus to design nonconformity measures that preserve this monotonicity under multi-condition settings, especially for intersection conditions, which we will address in the next section.

# 3.3 Error Accumulation in Two-Step cfBH Methods

However, these methods cannot guarantee FDR control, primarily due to error accumulation resulting from naive set operations. Such error propagation undermines their theoretical validity, necessitating a rigorously guaranteed approach for FDR control under multi-condition settings. We therefore present Corollary 3.1, supported by numerical results in Section 5.1 demonstrating the failure of both *Inter-cfBH* and *Union-cfBH*, thus providing empirical validation for the corollary.

**Corollary 3.1.** Applying two separate cfBH procedures [4] for boundary points and combining results via intersection (for the target interval  $(c_1, c_2)$ ) or union (for  $(-\infty, c_1) \cup (c_2, \infty)$ ) does not guarantee control of the false discovery rate at a prespecified level q, where  $c_1 < c_2$  are predefined thresholds.

**Remark 3.1** (Explanation for Corollary 3.1). For intersection selection  $S = S_1 \cap S_2$ , a false discovery requires simultaneous errors in both procedures. For instance, a unit with  $Y \leq c_1$  may be falsely selected if erroneously included by  $S_1$  yet retained by  $S_2$  (as  $Y \leq c_1 < c_2$ ). Similarly, for  $Y \geq c_2$ , error necessitates incorrect exclusion by  $S_2$  but correct inclusion by  $S_1$ . This multiplicative structure inflates FDR as S decreases, violating control guarantees. For union selection  $S = S_1 \cup S_2$ , errors accumulate additively. Units with  $Y_j \in [c_1, c_2]$  are falsely discovered if selected by either procedure. The numerator sums overlapping false discoveries, while correlation between  $S_1$  and  $S_2$  prevents proportional denominator growth, leading to FDR inflation. To address this, we then propose the following FDR-guaranteed method for Multi-Condition CS.

### 4 Proposed Method

In this section, we introduce the method with a finite-sample FDR guarantee for Multi-Condition CS. We begin by addressing conjunctive and disjunctive conditions, then introduce the complete *MCCS* for diverse logical combinations and extend it to multivariate response settings.

### 4.1 Addressing Conjunctive Conditions

Central to addressing conjunctive conditions (i.e.,  $c_1 < y < c_2$ ) is the design of the nonconformity score. For conjunctive conditions defined by the interval  $I_k = (c_{k_L}, c_{k_R})$ , the nonconformity score  $V^k(\mathbf{x}, \mathbf{y})$  in Algorithm 1 ensures regional monotonicity by leveraging the predictor  $\hat{\mu}(\mathbf{x})$  and a constant  $M > 2 \cdot \sup_x \max(c_{k_L} - \hat{\mu}(\mathbf{x}), \hat{\mu}(\mathbf{x}) - c_{k_R})$ . The score assigns  $M - \min(\hat{\mu}(\mathbf{x}) - c_{k_L}, c_{k_R} - \hat{\mu}(\mathbf{x}))$  if  $\mathbf{y} \in (c_{k_L}, c_{k_R})$ , and  $\max(c_{k_L} - \hat{\mu}(\mathbf{x}), \hat{\mu}(\mathbf{x}) - c_{k_R})$  otherwise, guaranteeing lower scores for samples within  $I_k$  to promote selection, while M ensures scores from interior points dominate exterior ones, enforcing monotonicity. The utility of M is further formalized in Proposition 4.1.

## Algorithm 1 Nonconformity Score for Conjunctive Conditions

```
1: function V^k(\mathbf{x}, \mathbf{y}) \Rightarrow For the determined interval I_k = (c_{k_L}, c_{k_R})

2: pred \leftarrow \hat{\mu}(\mathbf{x}), \quad M \leftarrow \text{constant} > 2 \cdot \sup_x \max(|c_{k_L} - \hat{\mu}(\mathbf{x})|, |\hat{\mu}(\mathbf{x}) - c_{k_R}|)

3: if \mathbf{y} > c_{k_L} and \mathbf{y} < c_{k_R} then return M - \min(pred - c_{k_L}, c_{k_R} - pred)

4: else return \max(c_{k_L} - pred, pred - c_{k_R})

5: end if

6: end function
```

**Proposition 4.1.** Let  $V^k$  be any fixed regionally monotone nonconformity score, and suppose  $\{(\mathbf{x}_i, \mathbf{y}_i)\}_{i=1}^{n+m}$  are exchangeable from distribution  $\mathcal{D}_{X\times Y}$ . Let  $(\mathbf{x},y)$  denote a random pair drawn from  $\mathcal{D}_{X\times Y}$ , and define F(v,u)= $\mathbb{P}(V^k(\mathbf{x}, \mathbf{y}) < v) + u \cdot \mathbb{P}(V^k(\mathbf{x}, \mathbf{y}) = v)$  for any  $v \in \mathbb{R}$  and  $u \in [0, 1]$ . For interval  $I_{Target} = I_k = (c_{k_L}, c_{k_R})$ , assuming fixed choice of  $\mathbf{c}_k \in I_k$ , define

$$t^* = \sup \left\{ t \in [0, 1] : \frac{t}{\mathbb{P}(F(V^k(\mathbf{x}, \mathbf{c}_k), U) \le t)} \le q \right\}.$$
 (5)

Suppose there exists  $t \in (t^* - \epsilon, t^*)$  such that  $\frac{t}{\mathbb{P}(F(V^k(\mathbf{x}, \mathbf{c}_k), U) \leq t)} \leq q$  for any sufficiently small  $\epsilon > 0$ . Then the output S of Algorithm 3 (where  $V^k$  adopts Algorithm 1) satisfies:

$$\lim_{n,m\to\infty} \text{FDR} = \frac{\mathbb{P}\left(F(V^k(\mathbf{x}, \mathbf{c}_k), U) \le t^*, \mathbf{y} \in I_k^c\right)}{\mathbb{P}\left(F(V^k(\mathbf{x}, \mathbf{c}_k), U) \le t^*\right)}, \quad and$$

$$\lim_{n,m\to\infty} \text{Power} = \frac{\mathbb{P}\left(F(V^k(\mathbf{x}, \mathbf{c}_k), U) \le t^*, \mathbf{y} \in I_k\right)}{\mathbb{P}(\mathbf{y} \in I_k)}.$$
(6)

Proposition 4.1 extends Proposition 7 in CS [4] from a single condition to conjunctive conditions, establishing the exact asymptotic behavior of both the FDR and power. The proof, being highly analogous, is omitted. Here, F(v,u) can be interpreted as a lower and more robust measure of evidence, while  $t^*$  corresponds to the critical threshold value selected by the BH procedure. The requirement that a small neighborhood around  $t^*$  satisfies the definition in (5) ensures stability in FDR control by excluding scenarios where  $t^*$  exhibits oscillatory behavior.

Under the assumption that  $V^k$  does not possess point masses, the meaning of  $t^*$  can be interpreted more intuitively by introducing  $v^*$ : let  $v^* = \sup \{v : P(V^k(X,Y) \le v) \le t^*\}$ , then the inequality in the definition of  $t^*$  in (5) can be rewritten as:

$$\frac{t^*}{\mathbb{P}(F(V^k(\mathbf{x}, \mathbf{c}_k), U) \le t^*)} = \frac{\mathbb{P}(V^k(\mathbf{x}, \mathbf{y}) \le v^*, \mathbf{y} \in I_k^c)}{\mathbb{P}(V^k(\mathbf{x}, \mathbf{c}_k) \le v^*)} \le \frac{\mathbb{P}(V^k(\mathbf{x}, \mathbf{y}) \le v^*)}{\mathbb{P}(V^k(\mathbf{x}, \mathbf{c}_k) \le v^*)} \le q$$
(7)

Hence, tightening the first inequality in (7) allows the algorithm to approach the nominal FDR more closely. The large constant M was introduced to achieve this objective, as detailed in Appendix A.2.

**Remark 4.1.** Although the "fixed choice" in Proposition 4.1 corresponds to a specific criterion, as in Theorem 4.1 of mCS [8], the criterion in Proposition 4.1 is defined by two conjunctive conditions rather than a single one in Theorem 4.1 of mCS [8]. Furthermore, Proposition 4.1 can be naturally extended to multivariate response settings with conjunctive conditions, which cannot be handled by Theorem 4.1 in [8].

# **Addressing Disjunctive Conditions**

Addressing disjunctive conditions (i.e.,  $y < c_1$  or  $y > c_2$ ) requires a more effective utilization of the BH procedure. To this end, we propose Algorithm 2, which implements via a global approach that aggregates all  $m \times \hat{K}$  p-values  $\mathcal{P} = \{p_j^k \mid j=1,\ldots,m; k=1,\ldots,K\}$ , sorts them ascendingly as  $p_{(1)} \leq \cdots \leq p_{(NUM)}$  where  $NUM = m \cdot K$ , finds the largest index  $l^*$  satisfying  $p_{(l^*)} \leq \frac{q \cdot l^*}{NUM}$ , and constructs the selection set  $\mathcal{S} = \left\{(j,k) : p_j^k \leq \frac{q \cdot l^*}{NUM}\right\}$ .

This method ensures finite-sample FDR control under exchangeability (Theorem 2.6, CS [4]) by integrating all hypotheses within a unified testing framework, thus particularly effective for selecting targets spanning multiple intervals as preventing the error inflation inherent in ad hoc combinations of separate cfBH procedures, and providing rigorous theoretical guarantees for FDR control under disjunctive conditions.

## Algorithm 2 Global BH Procedure

1: **procedure** GlobalBH( $\{p_i^k\}, q$ )

- $\triangleright j = 1, \dots, m; k = 1, \dots, K$
- 2:
- Collect all  $m \times K$  p-values:  $\mathcal{P} = \{p_j^k \mid j=1,\ldots,m; k=1,\ldots,K\}$ Sort p-values in ascending order:  $p_{(1)} \leq p_{(2)} \leq \cdots \leq p_{(NUM)}$  where  $NUM = m \cdot K$ 3:
- Find maximum  $l^*$  satisfying:  $p_{(l^*)} \leq \frac{q \cdot l^*}{NUM}$ 4:
- Construct selection set:  $\mathcal{S} = \left\{ (j,k) : p_j^k \leq \frac{q \cdot k^*}{NUM} \right\}$ 5:
- **return** Selection set  $\mathcal{S}$  $\triangleright$  Selected pairs (j,k) claiming  $\mathbf{y}_{n+j} \in I_k$  with FDR  $\leq q$ 6:
- 7: end procedure

### 4.3 Addressing More Combination Conditions

Building on the method for two-condition (conjunctive or disjunctive) CS, the approach can be extended to more formats and multi-condition combinations. A one-sided unbounded interval, defined by a single constraint, represents a special case of a conjunctive condition with one infinite threshold. Specifically, the nonconformity score for a left-unbounded interval  $I_k = (-\infty, c_{k_R})$  and a right-unbounded interval  $I_k = (c_{k_L}, +\infty)$  is defined respectively as:

$$V^{k}(\mathbf{x}, \mathbf{y}) = M \cdot \mathbf{1}_{\{\mathbf{y} < c_{k_{R}}\}} + \hat{\mu}(\mathbf{x}), \quad V^{k}(\mathbf{x}, \mathbf{y}) = M \cdot \mathbf{1}_{\{\mathbf{y} > c_{k_{L}}\}} - \hat{\mu}(\mathbf{x}).$$
(8)

Therefore, we propose the complement MCCS in Algorithm 2, which designs regionally monotone nonconformity scores  $V^k(\mathbf{x}, \mathbf{y})$  for each target interval  $I_k$ , computes conformal p-values  $p_j^k$  for all test samples and intervals based on the calibration data (as in Eq. (4)), and applies the global BH procedure as in Algorithm 2 to select all pairs (j, k), ensuring finite-sample FDR control.

## Algorithm 3 Multi-Condition Conformal Selection

To enhance practicality, we state Corollary 4.1, which establishes that overlapping intervals within  $I_{Target}$  preserve the exchangeability and conservativeness required for FDR control, as experimentally validated in Section 5.2. This property enables direct specification of multiple target intervals without explicit intersection checks. Theorem 4.1 formalizes the finite-sample FDR control guarantee of Algorithm 3, with proof provided in Appendix A.3.

**Corollary 4.1.** Under the conditions of Theorem 4.1, intersections among target intervals  $I_k$  do not affect the FDR control guaranteed by Algorithm 3.

**Theorem 4.1.** Suppose  $V^k$  is a regionally monotone nonconformity score, and for any  $j \in \{1, ..., m\}$ , the random variables  $V_1^k, ..., V_n^k, V_{n+j}^k$  are exchangeable conditioned on  $\{\widehat{V}_{n+\ell}^k\}_{\ell \neq j}$ . Then, for any  $q \in (0,1)$ , the output S of Algorithm 3 satisfies  $\mathrm{FDR} \leq q$ .

#### 4.4 Extension to Multivariate Response Settings

Building on mCS [8], Algorithm 3 extends naturally to multivariate responses. For conjunctive conditions, the target region is a bounded area  $\partial R$ ; for disjunctive conditions, Algorithm 4 is proposed, analogous to Algorithm 1. Algorithm 2 operates on conformal p-values independently of response dimension, enabling direct multivariate application. This integration generalizes MCCS for multivariate settings. See Appendix A.4 for details.

Algorithm 4 Nonconformity Score for Conjunctive Conditions under Multivariate Response Setting

```
1: function V^k(\mathbf{x}, \mathbf{y}) \triangleright For the determined region between \partial R_{inner} and \partial R_{outter}

2: \mathbf{pred} \leftarrow \hat{\mu}(\mathbf{x}), M \leftarrow \text{large constant}

3: if \mathbf{y} \notin R_{inner} and \mathbf{y} \in R_{outter} then

4: \mathbf{return} \ M - \min\{dis(\mathbf{pred}, \partial R_{inner}), dis(\mathbf{pred}, \partial R_{outter})\}

5: else return \max\{dis(\mathbf{pred}, \partial R_{inner}), dis(\mathbf{pred}, \partial R_{outter})\}

6: end if

7: end function
```

# 5 Experiments

We evaluated the method on both simulated and real-world data. Simulations demonstrated its superiority over baselines under conjunctive and disjunctive conditions, along with strong generalization to more complex conditional tasks. Real-world experiments confirmed its efficacy across various scenarios, including textual, visual, multimodal, and multi-class settings.

# 5.1 Compare with Baselines

**Experiments Setup.** We first perform numerical simulations using synthetically generated data. The covariates  $\mathbf{x}$  are sampled from  $\mathrm{Unif}(-10,10)^p$ , where  $\mathbf{p}$  denotes the dimension of  $\mathbf{x}$ . The response variable  $\mathbf{y}$  is generated by  $\mathbf{y} = \mu(\mathbf{x}) + \epsilon$ , where  $\mu$  represents the regression function and  $\epsilon$  denotes the random noise. An SVM with an RBF kernel is used for model fitting. The dataset is split into training, calibration, and test sets with a ratio of 8:1:1. Different experimental settings are constructed by varying the regression function and noise distribution. The FDP averaged over 1000 independent replications serves as the observed FDR.

Compared Baselines. We established the following baseline methods for comparison. The existing single-condition method was applied separately to each individual condition, and the resulting selection sets were combined using simple set operations: intersection (denoted as Int) and union (denoted as Uni). Bonferroni correction [14] versions of these procedures are referred to as Int-B and Uni-B, respectively. Additionally, Ind denotes an indicator method based on whether the response variable lies within the target region (i.e.,  $y_{Ind} > 0$  when  $\mathbf{y} \in I_{Target}$ ). Further details on settings and baselines are provided in Appendix B.

Table 1: Comparison with Baselines of Selection Performance for Conjunctive and Disjunctive Conditions under Univariate and Multivariate Response Settings (Optimal FDR control in **bold**).

#### (a) Conjunctive Conditions

#### (b) Disjunctive Conditions

	variate	Multi	Univariate		
Met	Power	FDR	Power	FDR	Method
Ui	0.9622	0.3531	0.9397	0.3766	Int
Uni	0.8549	0.2208	0.6005	0.1081	Int-B
In	0.1179	0.1491	0.2126	0.2013	Ind
MCCS	0.5348	0.2907	0.9756	0.2874	MCCS (Ours)

	Univariate		Multi	variate
Method	FDR	Power	FDR	Power
Uni	0.3766	0.9720	0.3165	0.8024
Uni- $B$	0.1569	0.9224	0.1644	0.5765
Ind	0.2290	0.0000	0.2172	0.0044
MCCS (Ours)	0.2848	0.9515	0.2628	0.7013

In Table 1, we compare the observed FDR and power with baseline methods, showing results for conjunctive conditions and disjunctive conditions at a nominal FDR level of 0.3. For the multivariate response setting, we report results with a response dimension of 30. As previously discussed, applying two separate single-condition methods followed by naive set operations leads to error accumulation, consistently yielding obtained FDR values above the nominal level. In contrast, the Bonferroni correction versions show an overly conservative behavior, underscoring the need for our proposed method. The *Ind* approach performs strongly, depending on the accuracy of the fitted model, often resulting in markedly low power. In comparison, our method robustly controls the FDR at or slightly below the nominal level while maintaining a relatively high power.

### 5.2 Experiments on More Combination Conditions

Table 2: Configuration of  $I_{Target}$  for Different Tasks.

Non-Intersecting Target Intervals	Intersecting Target Intervals
$\begin{array}{c} \textbf{Task 1:} & (-\infty,c_{1_R}) \cup (c_{2_L},c_{2_R}) \\ \textbf{Task 2:} & (c_{1_L},c_{1_R}) \cup (c_{2_L},+\infty) \\ \textbf{Task 3:} & (-\infty,c_{1_R}) \cup (c_{2_L},c_{2_R}) \cup (c_{3_L},c_{3_R}) \end{array}$	

We designed six different tasks, as shown in Table 3, including tasks with and without intersecting intervals, each task corresponding to a distinct form of  $I_{\text{Target}}$ . Table 3 presents the performance of MCCS on Task 5 across six distinct settings (STI-ST6) and three noise levels (Ns=0.1, 0.5, 0.9) at q=0.3. The results indicate a mild reduction

in power as noise increases; however, the method maintains robust performance across all configurations. Figure 2 presents the performance of MCCS under Setting 1 across six tasks at Ns=0.5 across varying nominal FDR levels q, ranging from 0.05 to 0.5 in increments of 0.05. Consistent with Corollary 4.1, intersecting target intervals does not compromise FDR control. Our method consistently maintains accurate FDR control while maintaining high power across all tasks.

**FDR** Power STNs=0.1Ns = 0.5Ns=0.5Ns=0.9Ns = 0.9Ns=0.10.2954 1 0.2971 0.2953 0.9548 0.9522 0.9502 2 0.2910 0.2912 0.2912 0.8630 0.8631 0.8623 3 0.2970 0.2969 0.2969 0.8843 0.8841 0.8841 4 0.2966 0.2963 0.2957 0.9530 0.9526 0.9483

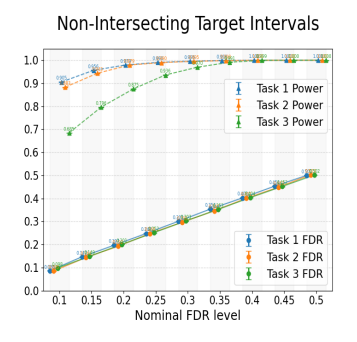
0.2915

0.2972

0.8632

0.8853

Table 3: Results across varying ST and Ns for Task5.



5

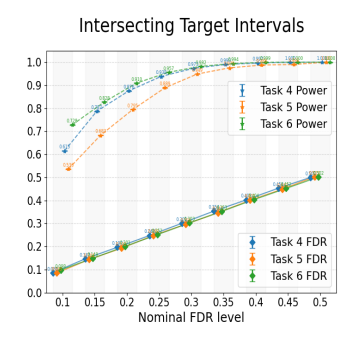
6

0.2913

0.2970

0.2912

0.2969



0.8628

0.8853

0.8630

0.8854

- (a) Results for Tasks 1-3.
- (b) Results for Tasks 4-6.

Figure 2: Results across varying q for Tasks 1-6.

### 5.3 Real Data Applications

Our method is applicable to diverse data types, as demonstrated in the following tasks, where the FDP from 500 independent replications serves as an estimate of the FDR.

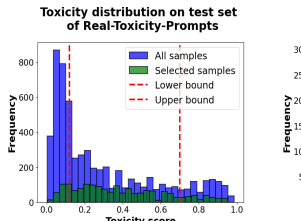
**NLP.** In natural language processing (NLP) tasks, we identify moderately toxic content for toxicity detection, aiming to prioritize manual review for moderate-risk cases, and automatically process high- and low-risk samples. Two datasets are used: *Real-Toxicity-Prompts* [15] (denoted as *nlp-A*) and *Pile-Toxicity-Balanced* [16, 17] (denoted as *nlp-B*).

**CV.** In computer vision (CV) tasks, we use the *NYU Depth Dataset V2* [18] to select samples within a specified depth interval. This approach introduces an important spatial prior that narrows the solution space, thereby enhancing measurement accuracy and robustness in the target domain. This can be implemented by excluding training samples that fall outside the desired bounds during dataset preparation. We employ two distinct models, *ResNet* [19] and *ViT* [20], for feature extraction, referred to as *cv-A* and *cv-B*, respectively.

In Table 4, we report the observed FDR and power for both the *nlp* and *cv* tasks at a nominal FDR level of 0.3. The results demonstrate that our method maintains effective FDR control tightly below the nominal level while achieving substantial power across varying

Table 4: Results on *nlp* and *cv* Tasks.

Task	FDR	Power
nlp-A	0.291	0.575
nlp-B	0.289	0.512
cv-A	0.261	0.892
cv-B	0.293	0.814



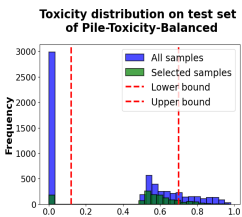


Figure 3: Visualization of *nlp*.

data modalities. Figure 3 visualizes the distribution of test set and selected samples in the *nlp* tasks, illustrating consistent performance across varying data structures. The selected samples remain concentrated in the target region, regardless of variations in the test set, highlighting the robustness of the approach.

**VQA.** We further evaluated our method on visual question answering (VQA) tasks incorporating both *nlp* and *cv* modalities using *VQA Dataset V2* [21]. The goal is to select test samples with predicted human agreement scores within a predefined confidence interval, focusing on moderately ambiguous instances that reflect partial consensus and are most suitable for model improvement and *human–AI* 

Table 5: Results on *vqa* Tasks.

Task	q	FDR	Power
vqa-A vqa-A	0.3 0.5	0.263 0.483	0.589 0.977
vqa-A vqa-B	0.3	0.485	0.726
vqa-B	0.5	0.477	0.991

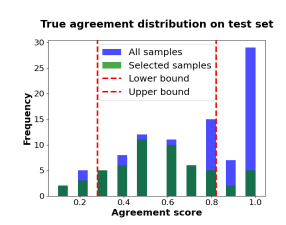


Figure 4: Visualization of vqa.

collaboration. We used *BLIP* [22] for confidence prediction, then predicted agreement using *Ridge* and *Bayesian-Ridge* (denoted as *vqa-A* and *vqa-B*). Table 5 reports the FDR and power achieved on the *vqa* tasks. Figure 4 illustrates the concentration in the target area of selected samples, confirming the selection's effectiveness. These results affirm the applicability of our method to multimodal contexts and indicate its potential for scalability to even larger models. Further details are provided in Appendix C.

**Multi-Class.** We extended our *MCCS* to multi-class tasks using the CIFAR-10 [23] and CIFAR-100 [24] datasets, enabling the selection of single, multiple, and similar classes. The achieved FDR closely aligns with the nominal FDR and maintains balanced class proportion during similar-class selection. Complete details are provided in Appendix D.

### 6 Related Work

Conformal Prediction (CP) [25, 26, 6] constructs prediction sets with finite-sample coverage guarantees under the assumption of exchangeability. Despite recent progress in CP [27, 28, 29, 30, 31, 32, 33], they cannot be directly applied to Conformal Selection (CS) problems, which require controlling FDR in a select set rather than constructing prediction sets with coverage guarantees. This gap motivated the development of the CS framework cfBH [4] to bridge CP principles with the selection tasks. Subsequent research has expanded this foundation into specialized extensions addressing diverse practical challenges. For instance, WCS [34] incorporates propensity score weighting to handle covariate shifts between calibration and test data, while mCS [8] generalizes the framework to multivariate responses, enabling selection based on multiple outcomes. For hierarchical data structures, conformal e-values [35] have been developed to ensure FDR control in settings with grouped data. Additionally, OptCS [36] enables data-driven model optimization without compromising validity, and ACS [37] dynamically updates the prediction model during the selection process to enhance power. DACS [38] integrates diversity metrics to promote representative selections, and a Neyman-Pearson-inspired approach [39] achieves asymptotic optimal power under covariate shift. Applications such as LLM alignment [7] and drug discovery [40] underscore the practical value of these advancements. However, these advances primarily focus on single-condition scenarios. Our work extends this line of research by addressing multi-condition settings while maintaining a theoretical guarantee, which is realistic in various real-world applications.

# 7 Conclusion

In this work, we introduce a theoretical extension of conformal selection to multi-condition settings, enabling reliable selection under multiple constraints. The proposed method overcomes the limitations of prior single-condition approaches by establishing rigorous finite-sample FDR control guarantees in multi-condition settings. Empirical validation across various domains confirms the practical effectiveness and adaptability of the approach, with extensions to multi-class scenarios, offering a versatile and theoretically grounded solution for selection in resource-limited scenarios.

**Limitations.** In line with standard conformal selection settings, the training and test data in our experiments were drawn from the same domain. However, domain shifts may occur in real-world applications, suggesting a direction for future research.

### **Ethics Statement**

This paper aimed to advance the field of Machine Learning. There are many potential societal consequences of our work, none of which we feel must be specifically highlighted here.

### References

- [1] F. Noor, M. Junaid, and A.H. et al. Almalki. Deep learning pipeline for accelerating virtual screening in drug discovery. *Scientific Reports*, 14:28321, 2024.
- [2] F. Hatib, Z. Jian, S. Buddi, C. Lee, J. Settels, K. Sibert, J. Rinehart, and M. Cannesson. Machine-learning algorithm to predict hypotension based on high-fidelity arterial pressure waveform analysis. *Anesthesiology*, 129:663–674, 2018.
- [3] John J. Cherian, Isaac Gibbs, and Emmanuel J. Candès. Large language model validity via enhanced conformal prediction methods. In *NeurIPS*, 2024.
- [4] Ying Jin and Emmanuel J. Candes. Selection by prediction with conformal p-values. *JMLR*, 2023.
- [5] Stephen Bates, Emmanuel J. Candès, Lihua Lei, Yaniv Romano, and Matteo Sesia. Testing for outliers with conformal p-values. *The Annals of Statistics*, 2023.
- [6] Vladimir Vovk, Alexander Gammerman, and Glenn Shafer. Algorithmic learning in a random world. 2005.
- [7] Yu Gui, Ying Jin, and Zhimei Ren. Conformal alignment: Knowing when to trust foundation models with guarantees. In *NeurIPS*, 2024.
- [8] Tian Bai, Yue Zhao, Xiang Yu, and Archer Y. Yang. Multivariate conformal selection. In ICML, 2025.
- [9] Michael D. Shultz. Two decades under the influence of the rule of five and the changing properties of approved oral drugs. *Journal of Medicinal Chemistry*, 2019.
- [10] Petre Lameski, Eftim Zdravevski, Saso Koceski, Andrea Kulakov, and Vladimir Trajkovik. Suppression of intensive care unit false alarms based on the arterial blood pressure signal. *IEEE Access*, 2017.
- [11] Sandeep Chandra Bollepalli, Rahul Kumar Sevakula, Wan-Tai M. Au-Yeung, Mohamad B Kassab, Faisal M. Merchant, George Bazoukis, Richard Boyer, Eric M. Isselbacher, and Antonis A. Armoundas. Real-time arrhythmia detection using hybrid convolutional neural networks. *Journal of the American Heart Association: Cardiovascular and Cerebrovascular Disease*, 2021.
- [12] Yoav Benjamini and Yosef Hochberg. Controlling the false discovery rate: a practical and powerful approach to multiple testing. *Journal of the Royal Statistical Society Series B-Methodological*, 1995.
- [13] Yoav Benjamini and Daniel Yekutieli. The control of the false discovery rate in multiple testing under dependency. *Annals of Statistics*, 2001.
- [14] Olive Jean Dunn. Multiple comparisons among means. *Journal of the American Statistical Association*, 1961.
- [15] Samuel Gehman, Suchin Gururangan, Maarten Sap, Yejin Choi, and Noah A. Smith. Realtoxicityprompts: Evaluating neural toxic degeneration in language models. In *Findings in EMNLP*, 2020.
- [16] Leo Gao, Stella Biderman, Sid Black, Laurence Golding, Travis Hoppe, Charles Foster, Jason Phang, Horace He, Anish Thite, Noa Nabeshima, Shawn Presser, and Connor Leahy. The Pile: An 800gb dataset of diverse text for language modeling. Technical report, EleutherAI, 2021.
- [17] Tomek Korbak. Pile-Toxicity-Balanced, 2023.
- [18] Nathan Silberman, Derek Hoiem, Pushmeet Kohli, and Rob Fergus. Indoor segmentation and support inference from rgbd images, 2012.
- [19] Kaiming He, Xiangyu Zhang, Shaoqing Ren, and Jian Sun. Deep residual learning for image recognition. In *CVPR*, 2016.
- [20] Alexey Dosovitskiy, Lucas Beyer, Alexander Kolesnikov, Dirk Weissenborn, Xiaohua Zhai, Thomas Unterthiner, Mostafa Dehghani, Matthias Minderer, Georg Heigold, Sylvain Gelly, Jakob Uszkoreit, and Neil Houlsby. An image is worth 16x16 words: Transformers for image recognition at scale. *arXiv preprint arXiv:2010.11929*, 2020.
- [21] Tsung-Yi Lin, Michael Maire, Serge Belongie, Lubomir Bourdev, Ross Girshick, James Hays, Pietro Perona, Deva Ramanan, C. Lawrence Zitnick, and Piotr Dollár. Visual Question Answering (VQA) v2.0 Validation Questions, 2017.

- [22] Junnan Li, Dongxu Li, Caiming Xiong, and Steven C. H. Hoi. Blip: Bootstrapping language-image pre-training for unified vision-language understanding and generation. In *ICML*, 2022.
- [23] Alex Krizhevsky, Vinod Nair, and Geoffrey Hinton. Learning multiple layers of features from tiny images, 2009. Dataset: CIFAR-10.
- [24] Alex Krizhevsky, Vinod Nair, and Geoffrey Hinton. Learning multiple layers of features from tiny images, 2009. Dataset: CIFAR-100.
- [25] Harris Papadopoulos. Inductive conformal prediction: Theory and application to neural networks. In *Tools in Artificial Intelligence*, 2008.
- [26] Vladimir Vovk. Conditional validity of inductive conformal predictors. Machine Learning, 2013.
- [27] Shayan Kiyani, George J. Pappas, and Hamed Hassani. Conformal prediction with learned features. In ICML, 2024.
- [28] Jiawei Ge, Debarghya Mukherjee, and Jianqing Fan. Optimal aggregation of prediction intervals under unsupervised domain shift. In NeurIPS, 2024.
- [29] Rui Luo and Zhixin Zhou. Conformity score averaging for classification. In ICML, 2025.
- [30] Jake C. Snell and Thomas L. Griffiths. Conformal prediction as bayesian quadrature. In ICML, 2025.
- [31] Shayan Kiyani, George J. Pappas, Aaron Roth, and Hamed Hassani. Decision theoretic foundations for conformal prediction: Optimal uncertainty quantification for risk-averse agents. In *ICML*, 2025.
- [32] Soroush H. Zargarbashi, Mohammad Sadegh Akhondzadeh, and Aleksandar Bojchevski. One sample is enough to make conformal prediction robust. In *NeurIPS*, 2025.
- [33] Maresa Schröder, Dennis Frauen, Jonas Schweisthal, Konstantin Heß, Valentyn Melnychuk, and Stefan Feuerriegel. Conformal prediction for causal effects of continuous treatments. In *NeurIPS*, 2025.
- [34] Ying Jin and Emmanuel J. Candès. Model-free selective inference under covariate shift via weighted conformal p-values. *ArXiv*, abs/2307.09291, 2023.
- [35] Yonghoon Lee and Zhimei Ren. Selection from hierarchical data with conformal e-values. *ArXiv*, abs/2501.02514, 2025.
- [36] Tian Bai and Ying Jin. Optimized conformal selection: Powerful selective inference after conformity score optimization. *ArXiv*, abs/2411.17983, 2024.
- [37] Yu Gui, Ying Jin, Yash Nair, and Zhimei Ren. Acs: An interactive framework for conformal selection. *ArXiv*, abs/2507.15825, 2025.
- [38] Yash Nair, Ying Jin, James Yang, and Emmanuel Candes. Diversifying conformal selections. *ArXiv*, abs/2506.16229, 2025.
- [39] Jing Qin, Yukun Liu, Moming Li, and Chiung-Yu Huang. Revamping conformal selection with optimal power: A neyman–pearson perspective. *ArXiv*, abs/2502.16513, 2025.
- [40] Tian Bai, Peng Tang, Yuting Xu, Vladimir Svetnik, Bingjia Yang, Abbas Khalili, Xiang Yu, and Archer Yang. Conformal selection for efficient and accurate compound screening in drug discovery. *ChemRxiv*, 2025.

# A Algorithm Details

## A.1 Explanation for FDR

We demonstrate that applying FDR control to each individual interval within a multi-interval target region ensures control of the overall FDR for samples falling outside all target intervals. For a specified target  $I_{Target}$ , if selection is performed for each interval  $I_k$ , one can readily show:

$$\begin{split} FDR_{Neither} = & E\left[\frac{claim: \mathbf{y}_{n+j} \in I_k, \quad but: \mathbf{y}_{n+j} \in I_{Target}^c}{1 \vee |\mathcal{S}|}\right] \\ \leq & E\left[\frac{claim: \mathbf{y}_{n+j} \in I_k, \quad but: \mathbf{y}_{n+j} \in I_k^c}{1 \vee |\mathcal{S}|}\right] = FDR, \end{split}$$

Hence, maintaining FDR control for any individual interval  $I_k$  suffices to control the overall FDR across all intervals. Therefore, we subsequently focus on controlling the FDR for each interval.

### A.2 Explanation for The Large Constant M

Tightening the first inequality in (7) can be achieved by ensuring  $V^k(\mathbf{x},\mathbf{y}) \leq v^*$  so that  $\mathbf{y} \notin I_k$ . In an extreme case,  $V^k(\mathbf{x},\mathbf{y})$  can be defined as  $-\hat{\mu}(\mathbf{x})$  when  $\mathbf{y} \notin I_k$  and  $+\infty$  when  $\mathbf{y} \in I_k$ . As a practical compromise, we define  $V(x,y) = M \cdot \mathbf{1}_{\{\mathbf{y} \in I_k\}} - \min \left(\hat{\mu}(\mathbf{x}) - c_{k_L}, \ c_{k_R} - \hat{\mu}(\mathbf{x})\right)$ , where  $M > 2 \cdot \sup_x \max(|c_{k_L} - \hat{\mu}(\mathbf{x})|, |\hat{\mu}(\mathbf{x}) - c_{k_R}|)$ , which leads to:

$$\begin{split} V^k(\mathbf{x}, \mathbf{y}_{\text{where } \mathbf{y} \in I_k)} \geq & 2 \cdot \sup_{x} \max(\left| c_{k_L} - \hat{\mu}(\mathbf{x}) \right|, \left| \hat{\mu}(\mathbf{x}) - c_{k_R} \right|) - \min\left( \hat{\mu}(\mathbf{x}) - c_{k_L}, \ c_{k_R} - \hat{\mu}(\mathbf{x}) \right) \\ \geq & 2 \cdot \sup_{x} \max(\left| c_{k_L} - \hat{\mu}(\mathbf{x}) \right|, \left| \hat{\mu}(\mathbf{x}) - c_{k_R} \right|) - \max\left(\left| \hat{\mu}(\mathbf{x}) - c_{k_L} \right|, \ \left| c_{k_R} - \hat{\mu}(\mathbf{x}) \right| \right) \\ \geq & \sup_{x} \max(\left| c_{k_L} - \hat{\mu}(\mathbf{x}) \right|, \left| \hat{\mu}(\mathbf{x}) - c_{k_R} \right|) \\ \geq & V^k(\mathbf{x}, \mathbf{y}_{\text{where } \mathbf{y} \notin I_k}), \end{split}$$

This ensures that the nonconformity scores for  $\mathbf{y} \in I_k$  are always larger than those for  $\mathbf{y} \notin I_k$ . When  $q < \mathbb{P}(\mathbf{y} \notin I_k)$ , it follows from the definition that  $v^*$  lies below the q-th quantile of  $V^k(\mathbf{x}, \mathbf{y})$ . Consequently, the first inequality in (7) becomes an exact equality, leading to obtaining an FDR closer to the nominal level and a higher power.

For multivariate response settings, the absolute difference should be replaced by a distance metric, i.e.,  $M > 2 \cdot \sup_x \max(dis(\hat{\mu}(\mathbf{x}), \partial R_{inner}), dis(\hat{\mu}(\mathbf{x}), \partial R_{outter})$ , where R is the target region, and  $dis(\hat{\mu}(\mathbf{x}), \partial R) = \inf_{\mathbf{r} \in R^c} \|\hat{\mu}(\mathbf{x}) - \mathbf{r}\|_p$ .

# A.3 Proof of Theorem 4.1

**Exchangeability Condition.** Given the *i.i.d.* data and fixed model, for any fixed (j,k), the random variables  $V_1^k,\ldots,V_n^k,V_{n+j}^k$  are exchangeable. More precisely, conditional on the estimated test scores  $\{\widehat{V}_{n+\ell}^h:\ell\neq j,h=1,\ldots,K\}$ , these scores are exchangeable. This is because the calibration scores are based on *i.i.d.* data, and the true test score  $V_{n+j}^k$  comes from the same distribution. Conditioning on the estimated scores of other test points does not affect exchangeability, as these estimates are based on independent test points and a fixed model.

Consequently, for any null hypothesis  $(j,k) \in \mathcal{H}_0$ , the oracle p-value  $p_j^{k*}$  is superuniform conditional on the other p-values. That is, for any  $t \in [0,1]$ ,  $\mathbb{P}(p_j^{k*} \leq t \mid \mathcal{F}_{-j,-k}) \leq t$ , where  $\mathcal{F}_{-j,-k}$  is the  $\sigma$ -algebra generated by all other p-values, i.e.,  $\{p_l^h: (l,h) \neq (j,k)\}$ .

**Properties of the BH Procedure.** The BH procedure has key properties used in the proof. Let  $R = |\mathcal{S}|$ , and  $R_{-j,-k} = |\mathcal{S}_{-j,-k}|$ , where  $\mathcal{S}_{-j,-k}$  is the selection set obtained by applying the BH procedure to all p-values except  $p_j^k$ . Then,  $R \geq R_{-j,-k}$  because adding a p-value cannot decrease the number of rejections. Moreover, if  $p_j^k > \frac{q \cdot R_{-j,-k}}{NUM}$ , then adding  $p_j^k$  does not change the rejection count, so  $R = R_{-j,-k}$ . These properties are standard and are utilized in the proof.

**Proof of Theorem 4.1.** We now prove that under the exchangeability condition and regional monotonicity, the *MCCS* algorithm controls FDR  $\leq q$ .

Begin by decomposing the FDR:

$$FDR = \mathbb{E}\left[\frac{|\mathcal{S} \cap \mathcal{H}_0|}{|\mathcal{S}| \vee 1}\right] = \sum_{(j,k) \in \mathcal{H}_0} \mathbb{E}\left[\frac{\mathbf{1}\{(j,k) \in \mathcal{S}\}}{|\mathcal{S}|}\right],$$

since for  $(j,k) \in \mathcal{H}_0$ ,  $\mathbf{1}\{(j,k) \in \mathcal{S} \text{ and } \mathbf{y}_{n+j} \notin I_k\} = \mathbf{1}\{(j,k) \in \mathcal{S}\}.$ 

Let  $R = |\mathcal{S}|$ ,  $NUM = m \cdot K$ . For any  $(j,k) \in \mathcal{H}_0$ , the event  $(j,k) \in \mathcal{S}$  is equivalent to  $p_j^k \leq \frac{g \cdot R}{NUM}$  by the definition of the BH procedure. Thus,

$$\mathbb{E}\left[\frac{\mathbf{1}\{(j,k)\in\mathcal{S}\}}{R}\right] = \mathbb{E}\left[\frac{\mathbf{1}\{p_j^k \leq \frac{q\cdot R}{NUM}\}}{R}\right].$$

Since  $\mathbf{y}_{n+j} \notin I_k$ , regional monotonicity implies  $p_i^{k*} \leq p_i^k$ , so

$$\mathbf{1}\{p_j^k \le \frac{q \cdot R}{NUM}\} \le \mathbf{1}\{p_j^{k*} \le \frac{q \cdot R}{NUM}\},\,$$

and hence

$$\mathbb{E}\left[\frac{\mathbf{1}\{p_j^k \leq \frac{q \cdot R}{NUM}\}}{R}\right] \leq \mathbb{E}\left[\frac{\mathbf{1}\{p_j^{k*} \leq \frac{q \cdot R}{NUM}\}}{R}\right].$$

Now, introduce conditional expectation. Let  $\mathcal{F}_{-j,-k}$  be the  $\sigma$ -algebra generated by all p-values except  $p_j^k$ . Let  $R_{-j,-k}$  be the number of rejections when applying the BH procedure to all p-values except  $p_j^k$ . By the properties of the BH procedure,  $R \geq R_{-j,-k}$ , and if  $p_j^k > \frac{q \cdot R_{-j,-k}}{NUM}$ , then  $R = R_{-j,-k}$ . Therefore,

$$\frac{\mathbf{1}\{p_j^k \leq \frac{q \cdot R}{NUM}\}}{R} \leq \frac{\mathbf{1}\{p_j^k \leq \frac{q \cdot R_{-j,-k}}{NUM}\}}{R_{-j,-k}}.$$

This holds because if  $p_j^k \leq \frac{q \cdot R - j, -k}{NUM}$ , then since  $R \geq R_{-j,-k}$ , we have  $\frac{q \cdot R}{NUM} \geq \frac{q \cdot R - j, -k}{NUM}$ , so  $p_j^k \leq \frac{q \cdot R}{NUM}$ , and  $\frac{1}{R} \leq \frac{1}{R_{-j,-k}}$  (as  $R \geq R_{-j,-k} > 0$ ), making the left side less than or equal to the right side. If  $p_j^k > \frac{q \cdot R_{-j,-k}}{NUM}$ , the right side is zero, and  $R = R_{-j,-k}$  implies the left side is also zero.

Thus,

$$\mathbb{E}\left\lceil\frac{\mathbf{1}\{p_j^k \leq \frac{q \cdot R}{NUM}\}}{R}\right\rceil \leq \mathbb{E}\left\lceil\frac{\mathbf{1}\{p_j^k \leq \frac{q \cdot R_{-j,-k}}{NUM}\}}{R_{-j,-k}}\right\rceil.$$

Since  $p_i^{k*} \leq p_i^k$ , we have

$$\mathbf{1}\{p_j^k \le \frac{q \cdot R_{-j,-k}}{NUM}\} \le \mathbf{1}\{p_j^{k*} \le \frac{q \cdot R_{-j,-k}}{NUM}\},$$

so

$$\mathbb{E}\left\lceil\frac{\mathbf{1}\{p_j^k \leq \frac{q \cdot R_{-j,-k}}{NUM}\}}{R_{-j,-k}}\right\rceil \leq \mathbb{E}\left\lceil\frac{\mathbf{1}\{p_j^{k*} \leq \frac{q \cdot R_{-j,-k}}{NUM}\}}{R_{-j,-k}}\right\rceil.$$

Next, apply superuniformity. Conditional on  $\mathcal{F}_{-j,-k}$ ,  $R_{-j,-k}$  is fixed, and  $p_j^{k*}$  is superuniform:

$$\mathbb{P}(p_j^{k*} \le t \mid \mathcal{F}_{-j,-k}) \le t \quad \text{for any } t \in [0,1].$$

Therefore,

$$\mathbb{E}\left[\frac{1\{p_j^{k*} \le \frac{q \cdot R_{-j,-k}}{NUM}\}}{R_{-j,-k}} \mid \mathcal{F}_{-j,-k}\right] \le \frac{q \cdot R_{-j,-k}/NUM}{R_{-j,-k}} = \frac{q}{NUM}.$$

Taking expectation,

$$\mathbb{E}\left\lceil \frac{\mathbf{1}\{p_j^{k*} \leq \frac{q \cdot R_{-j,-k}}{NUM}\}}{R_{-j,-k}}\right\rceil \leq \frac{q}{NUM}.$$

Combining the inequalities,

$$\mathbb{E}\left[\frac{\mathbf{1}\{p_j^k \leq \frac{q \cdot R}{NUM}\}}{R}\right] \leq \frac{q}{NUM}.$$

Finally, sum over all null hypotheses:

$$\mathrm{FDR} = \sum_{(j,k) \in \mathcal{H}_0} \mathbb{E}\left[\frac{\mathbf{1}\{(j,k) \in \mathcal{S}\}}{R}\right] \leq \sum_{(j,k) \in \mathcal{H}_0} \frac{q}{NUM} = q \cdot \frac{|\mathcal{H}_0|}{NUM} \leq q,$$

since  $|\mathcal{H}_0| \leq NUM$ .

# A.4 Details of the Extension to Multivariate Response Settings

The MCCS algorithm can be naturally extended to multivariate response settings, where the target region may comprise multiple domains bounded by several constraints. For brevity, we term this generalized approach Multi-Region Conformal Selection (MRCS). Analogous to Algorithm 3, we provide the complete procedure for MRCS below, where  $dis(\hat{\mu}(\mathbf{x}), \partial R) = \inf_{\mathbf{r} \in R^c} \|\hat{\mu}(\mathbf{x}) - \mathbf{r}\|_p$ , and project denotes a mapping function used to derive the expression for  $\mathbf{y}$  from the boundary equation of region  $\partial R$  for computation of the nonconformity scores of test samples.

## Algorithm 5 Multi-Region Conformal Selection

```
Input: \mathcal{D}_{\text{calib}} = \{(\mathbf{x}_i, \mathbf{y}_i)\}_{i=1}^n, \{\mathbf{x}_{n+j}\}_{j=1}^m, \{R_k\}_{k=1}^K \text{ (with boundary equations), } q \in (0,1), \hat{\mu}(\cdot) \text{ (pre-trained predictor), } M > 2 \cdot \sup_x \max(dis(\hat{\mu}(\mathbf{x}), \partial R_{inner}), dis(\hat{\mu}(\mathbf{x}), \partial R_{outter})
         for k \leftarrow 1 to K do
                                                                                                                                                                         ▶ Region-specific nonconformity scores
                  if R_k has inner boundary \partial R_k^{\text{inner}} then Define V^k(x,\mathbf{y}) = M \cdot \mathbf{1}\{\mathbf{y} \in R_k\} - dis(\hat{\mu}(x), \partial R_k^{\text{inner}})
   2:
   3:
   4:
                  if R_k has outer boundary \partial R_k^{	ext{outer}} then Define V^k(x,\mathbf{y}) = M \cdot \mathbf{1}\{\mathbf{y} \in R_k\} + dis(\hat{\mu}(x),\partial R_k^{	ext{outer}})
   5:
   6:
   7:
                  if R_k has both boundaries then
   8:
                           \text{Define } V^k(\hat{\mu}(\mathbf{x}), \mathbf{y}) = \begin{cases} M - \min\{dis(\hat{\mu}(\mathbf{x}), \partial R_k^{\text{inner}}), dis(\hat{\mu}(\mathbf{x}), \partial R_k^{\text{outer}})\} & \mathbf{y} \in R_k \\ -\max\{dis(\hat{\mu}(\mathbf{x}), \partial R_k^{\text{inner}}), dis(\hat{\mu}(\mathbf{x}), \partial R_k^{\text{outer}})\} & \mathbf{y} \notin R_k \end{cases}
   9:
 10:
                   end if
 11: end for
 12: for k \leftarrow 1 to K and i \leftarrow 1 to n do
                                                                                                                                                                                                  > Compute calibration scores
                  V_i^k \leftarrow V^k(\mathbf{x}_i, \mathbf{y}_i)
 14: end for
 15: for k \leftarrow 1 to K and j \leftarrow 1 to m do
                                                                                                                                                                                    \triangleright Compute test scores and p-values
                  \mathbf{b}_k \leftarrow \operatorname{project}(\partial R_k) \;, \quad \widehat{V}_j^k \leftarrow V_k(\mathbf{x}_j, \mathbf{b}_k) Then construct p_j^k as in (4)
 18: end for
19: \mathcal{P} \leftarrow \operatorname{sort}\left(\left\{p_{j}^{k}\right\}_{j=1,k=1}^{m,K}\right), l^{*} \leftarrow \max\left\{l: \mathcal{P}[l] \leq \frac{q \cdot l}{m \cdot K}\right\}.
                                                                                                                                                                                                               ⊳ Global BH procedure
Output: Selection set S = \left\{ (j,k) : p_j^k \le \frac{q \cdot l^*}{m \cdot K} \right\}.
```

### A.5 Additional Explanation

In Algorithm 2 and Algorithm 5, when M is large, the subtracted term becomes negligible and can be omitted. Similarly, calibration samples outside the target selection have minimal influence and may also be excluded, thereby conserving computational resources.

### **B** Details of Numerical Experiments

## **B.1** Data Generating Processes for Univariate Responses Settings

The synthetic datasets are systematically constructed to evaluate methodological performance under controlled conditions with varying degrees of complexity, encompassing a spectrum from linear to highly nonlinear

relationships paired with different noise characteristics. Settings 1-3 are designed with distinct functional structures: Setting 1 embodies a linear data-generating mechanism, Setting 2 introduces moderate nonlinearity through a combination of exponential and trigonometric components, and Setting 3 further increases model intricacy with multi-feature nonlinear interactions.

To rigorously assess robustness under different stochastic environments, Settings 4-6 adopt the same functional relationships as Settings 1-3, respectively, but incorporate Laplacian noise instead of Gaussian noise, thereby introducing heavy-tailed disturbances that present additional modeling challenges. Across all configurations, independent noise, Gaussian in Settings 1-3 and Laplacian in Settings 4-6, is added with zero mean and comparable variance, which corresponds to the noise level varying in Section 5.2, to ensure equitable comparison of noise resilience. Detailed mathematical formulations for each setting are explicitly provided in Table 6, enabling a transparent and reproducible evaluation of model behavior under diverse data-generating processes and noise regimes.

Setting	$\mu(\mathbf{x})$	$\epsilon$
1	$\sum_{j=1}^p \beta_j x_j$ with $\beta_j \sim \mathcal{N}(0,1)$	$\mathcal{N}(0, \sigma^2)$
2	$\exp(x_1) + \sin(\pi \cdot x_2)$	$\mathcal{N}(0,\sigma^2)$
3	$\exp(x_1) + \sin(\pi \cdot x_2) + \exp(x_3) + \sin(\pi \cdot x_4) + \exp(x_5) + \sin(\pi \cdot x_6)$	$\mathcal{N}(0,\sigma^2)$
4	Same as Setting 1	$\mathcal{L}(0,\lambda)$
5	Same as Setting 2	$\mathcal{L}(0,\lambda)$
6	Same as Setting 3	$\mathcal{L}(0,\lambda)$

Table 6: True regression functions and noise distributions

#### **B.2** Details of the Baseline Method *Ind*

The method provides a unified algebraic approach to transform the geometric condition of whether a point lies within one or multiple target regions into an equivalent analytical condition expressed via the sign of a scalar-valued function.

In the univariate case, the target set consists of intervals, such as  $(a,b) \cup (c,d)$ . A polynomial function f(t) is constructed as the negative product of shifted linear factors:

$$f(t) = -(t - a)(b - t)(t - c)(d - t).$$

A point Y belongs to the union of the intervals if and only if f(Y) > 0. This criterion converts the set-membership condition into an inequality constraint amenable to algorithmic evaluation.

The multivariate extension, take 2-dimension as an instance, generalizes this idea to multiple curved regions—each defined by a quadratic inequality of the form  $(x-h_i)^2+(y-k_i)^2< r_i^2$ . The overall target region is defined by Boolean combinations of such inequalities. The function f(u,v) is constructed as the negative product of the left-hand sides of these quadratic expressions:

$$f(u,v) = -\prod_{i=1}^{m} \left[ (u - h_i)^2 + (v - k_i)^2 - r_i^2 \right].$$

Then, a point  $Y = (Y_1, Y_2)$  lies within the target region if and only if  $f(Y_1, Y_2) > 0$ . This construction effectively encodes the geometry of multiple intersecting circles into a single differentiable function whose sign indicates membership.

This method offers a computationally tractable approach to transform geometric constraints into algebraic inequalities applicable to both univariate and multivariate response settings. However, its performance is often suboptimal due to a strong dependence on the accuracy of  $\mu(\mathbf{x})$ .

#### **B.3** Details of Tasks in Section 5.2

We constructed six distinct tasks in Section 5.2, encompassing both scenarios with intersecting target intervals and those without overlaps. To detail the experimental parameters and offer a schematic overview, Figure 5 is provided below.

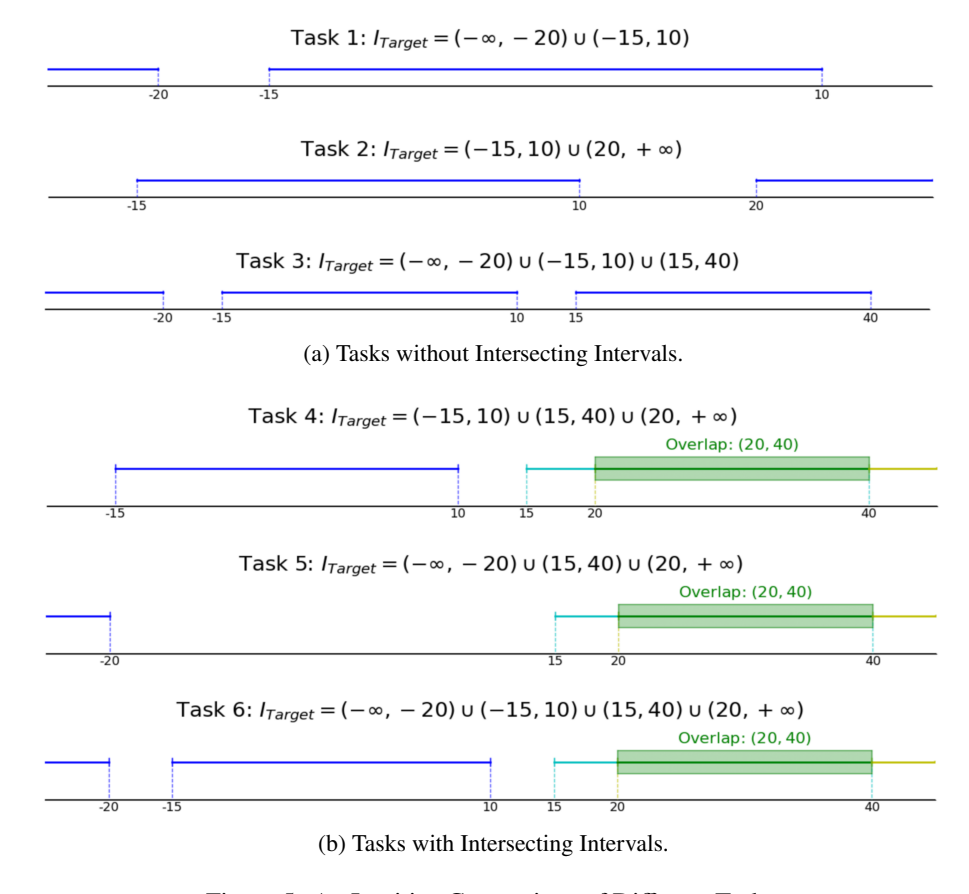


Figure 5: An Intuitive Comparison of Different Tasks.

### **B.4** Details of Multivariate Response Settings

**Data Generation.** We use a dataset generation function to produce multivariate regression data with systematically controlled feature-response relationships and correlated noise structures. It enables the evaluation of multidimensional regression methods under varying conditions of dimensionality and noise correlation. For each observation, the predictor variables  $\mathbf{x}$  are uniformly sampled from the interval [-1, 1], forming an  $n \times d$  design matrix where d denotes the feature dimension (default 5). The response matrix  $\mathbf{y} \in \mathbb{R}^{n \times k}$  is constructed through a structured linear combination: each dimension  $Y_i$  is generated as  $y_i = 2 \cdot x_j - 0.5 \cdot x_{j+1} + x_{j+2} + 1.5$ , with  $j = i \mod d$ . This results in a rotating feature selection pattern across response dimensions, establishing a consistent yet varied linear relationship between predictors and responses.

To emulate realistic correlated noise, multivariate Gaussian noise is introduced via a covariance matrix  $\Sigma$  with a specific structure: all diagonal elements are equal, and all off-diagonal elements are also equal, reflecting a homogeneous variance and uniform correlation across all response dimensions. Here,  $\sigma$  controls the overall noise level and  $\rho$  sets the magnitude of correlation between any two dimensions. This setup allows fine-grained control over both the signal-to-noise ratio and the inter-dimensional correlation pattern. The data generation strategy supports rigorous evaluation of regression methods across several key aspects: the number of response variables k, the noise intensity  $\sigma$ , the correlation strength  $\rho$ , and the predictor dimension d, providing a transparent and reproducible framework for assessing model performance under controlled settings.

**Task Settings.** We define the conjunctive conditions for multivariate responses as a ring-shaped region centered at  $(2,2,\ldots,2)$  across all dimensions, forming a symmetric reference frame. This annular region is bounded by two concentric hyperspheres whose radii are scaled proportionally from a predefined dimension-specific base value. A point is considered within the region if its Euclidean distance to the center lies between 0.6 and 1.0 times the reference radius, thus creating a well-defined annular subspace for conjunctive conditions under multivariate settings.

We define the disjunctive conditions for multivariate responses as a multi-sphere region, constructed from several hyperspheres, each with distinct centers and radii. The primary sphere is centered at  $(2, 2, \ldots, 2)$ , while subsequent spheres are displaced via controlled random offsets uniformly sampled from  $[-0.5, 0.5]^d$ , with offsets growing proportionally to the sphere index. The radii increase gradually from 80% of the base value, thus forming a cluster of intersecting hyperspheres with systematically varying positions and sizes that produce complex overlapping regions suitable for evaluating multivariate methods for disjunctive conditions.

Based on the aforementioned framework, we performed a series of simulation studies with response dimensions set to d=10,30, and 50. The corresponding radii used in each configuration are summarized in Table 7. In these configurations, the task involving the union of conditions is referred to as *Spherical Shell*; we provide the outer sphere radius, while the inner sphere radius is set to 0.6 times the outer radius, as described earlier. For the union of multiple spherical conditions, experiments were conducted with varying numbers  $num_{sp}=2,4$ , and 8 of spheres, and the reference sphere radius is reported for each case.

Task	d = 10	d = 30	d = 50
Spherical Shell	5.1	8.1	10.5
2 Spheres	4.4	7.1	8.9
4 Spheres	4.4	7.2	9.5
8 Spheres	4.9	8.2	10.5

Table 7: Radius Settings for Multivariate Tasks with Varying Dimensionality of y.

**More Results.** Under the experimental framework outlined above, which aligns with the univariate configuration, we employed an SVR model with an RBF kernel as the regression method. The observed FDR was estimated by averaging the FDP over 100 repeated experimental trials. In this section, we present a more comprehensive set of results than those discussed in Section 5.

For the conjunctive conditions, we compared our approach with a baseline method, denoted as *Int*, which directly applies the intersection of two single-condition selection procedures. The experimental outcomes, summarized in Table 8, reveal that our method consistently achieves effective FDR control across varying response dimensions. In contrast, the *Int* baseline consistently produced FDR values exceeding the nominal level, underscoring the deficiency in its theoretical guarantees. Although the *Int* method occasionally attained higher statistical power than our approach, this apparent advantage came at the expense of a loss in FDR control. It is important to note that pursuing higher power alone, for instance, by selecting all samples, is trivial and statistically uninformative. Hence, the ability to maintain high power under strict FDR constraints represents a meaningful and advantageous property of our method.

Table 8: Comparison with Baseline of Selection Performance for Conjunctive Conditions under Multivariate Response Settings (Optimal FDR control in **bold**).

D: : C	FDR		Po	wer
Dimension of y	Int	MCCS	Int	MCCS
d=10	0.3534	0.2998	0.9696	0.8878
d=30	0.4195	0.2940	0.9761	0.4737
d=50	0.3469	0.2931	0.9787	0.6338

For the disjunctive conditions, we compared our approach with a baseline method denoted as *Uni*, which simply applies the union of two single-condition selection procedures. Experiments were conducted across varying response dimensions, each involving target sets composed of different numbers of spheres. The results, summarized in Table 9, demonstrate that our method consistently maintains effective FDR control with relatively high power under all dimensional and number of spheres settings. In contrast, the *Uni* baseline consistently produced FDR values exceeding the nominal threshold, underscoring the inherent limitations of such heuristic strategies due to error propagation and affirming the theoretical soundness of our proposed approach.

Table 9: Comparison with Baseline of Selection Performance for Disjunctive Conditions under Multivariate Response Settings (Optimal FDR control in **bold**).

(a)	$num_{sn}$	=	2
(u)	rewritesp		_

D: : 6	FI	OR	Po	wer
Dimension of y	Uni	MCCS	Uni	MCCS
d=10	0.3079	0.2679	0.7641	0.6977
d=30	0.3164	0.2788	0.7611	0.7718
d=50	0.3133	0.2833	0.7484	0.7794

(b) 
$$num_{sp} = 4$$

Dimension	FDR		Power	
Dimension of y	Uni	MCCS	Uni	MCCS
d=10	0.3125	0.2683	0.7584	0.6759
d=30	0.3178	0.2822	0.7877	0.7236
d=50	0.3094	0.2751	0.8512	0.7905

(c) 
$$num_{sp} = 8$$

D:	FI	FDR		wer
Dimension of y	Uni	MCCS	Uni	MCCS
d=10	0.3159	0.2791	0.7614	0.6663
d=30	0.3172	0.2706	0.7964	0.6438
d=50	0.3166	0.2636	0.8199	0.6305

# C Details of Real Data Application

# C.1 Details of Tasks of cv

The *cv* tasks employ a pipeline for monocular depth estimation from RGB images, utilizing pre-trained ResNet and ViT models, respectively. This is combined with the *MCCS* approach based on conformal inference to identify samples falling within a specified target depth interval.

Experiments are conducted on the NYU Depth V2 dataset, which comprises 1,449 RGB-D images of indoor scenes along with depth maps captured using a Microsoft Kinect sensor. Each image has a resolution of  $640 \times 480$  pixels, with depth values representing physical distances in meters. The dataset is partitioned into training (74%), calibration (13%), and test (13%) sets. Depth values are obtained by averaging the center crop of each depth map, resulting in a single scalar depth value per image. We then use a Ridge regressor to predict the depth for the following steps.

To intuitively demonstrate the applicability of our proposed method on cv tasks, Figure 6 illustrates the implementation workflow of the algorithm across different aspects of the dataset. The visualization component provides critical diagnostic and interpretive tools for evaluating the method's performance: 1) The p-value distribution histogram assesses conformity to uniform distribution assumptions under the null hypothesis; 2) The Benjamini-Hochberg procedure plot illustrates the relationship between sorted p-values and the critical threshold line, demonstrating the selection mechanism that controls false discoveries; 3) Depth distribution histograms contrast selected versus unselected samples, revealing how effectively the method identifies targets within the specified interval; 4) The prediction-versus-truth scatterplot visualizes regression accuracy while highlighting correct/incorrect selections relative to the interval boundaries. These visualizations collectively offer an assessment

of both statistical properties (FDR control validity) and operational characteristics (depth estimation accuracy), enabling a comprehensive evaluation of the *MCCS*'s effectiveness in identifying samples within the target depth range. Figure 7 shows samples selected in the *cv* tasks.

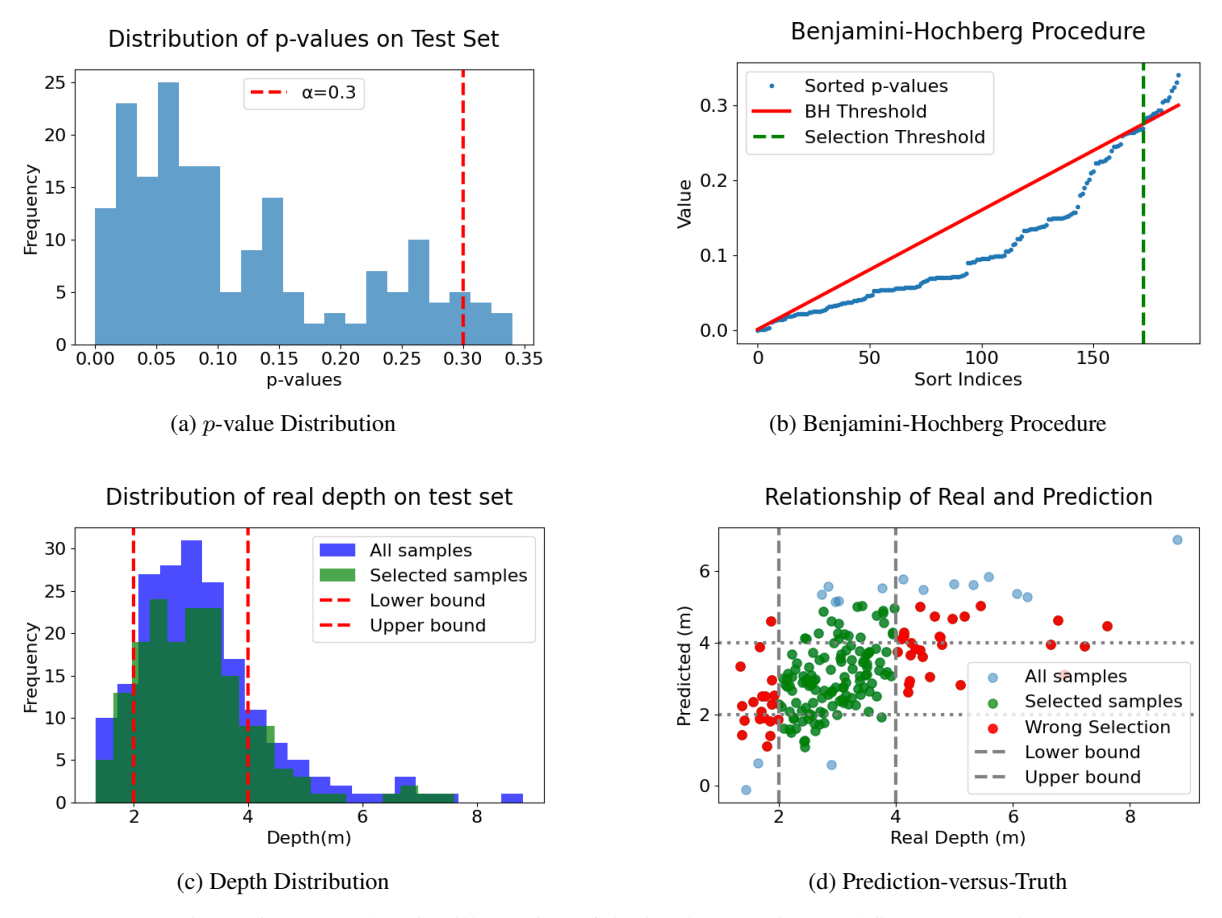


Figure 6: Comprehensive illustration of the implementation workflow on cv tasks.

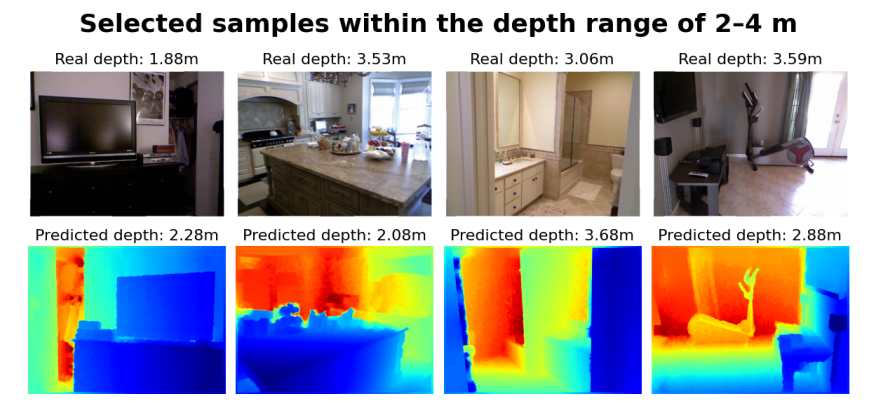


Figure 7: Selected Samples in the cv Tasks.

### C.2 Details of Tasks of *nlp*

The *nlp* tasks employ a conformal prediction pipeline with FDR control to identify text prompts within a target toxicity range. Using text embeddings and regression models, toxicity scores are predicted; the *MCCS* method then selects samples within the desired interval (e.g., (0.12, 0.7)) while controlling errors. Applied to the

Real-Toxicity-Prompts and Pile-Toxicity-Balanced datasets, the framework encompasses data loading, feature extraction via sentence embeddings, regression, nonconformity scoring, and the Benjamini–Hochberg procedure.

The Real-Toxicity-Prompts dataset contains 100K online texts, each annotated with continuous toxicity scores (0–1) from Perspective API, capturing diverse real-world language use. The Pile-Toxicity-Balanced subset includes 40K text segments from The Pile, with balanced binary toxicity labels (50% toxic / 50% non-toxic) achieved through stratified sampling to mitigate class imbalance. Together, these datasets support robust toxicity detection: the first enables fine-grained analysis of real-world toxicity, while the second ensures equitable evaluation via controlled class distribution.

The datasets are split via stratified sampling into training (60%), calibration (20%), and test (20%) sets to preserve toxicity distributions. For efficiency, up to 30,000 prompts are subsampled while maintaining score distribution. Text embeddings are generated using MiniLM-L6 (384-dimensional), a lightweight transformer, and used as features in a Ridge regression model trained only on the training set, with calibration and test sets reserved for subsequent steps. Figures 8 and 9 intuitively demonstrate our method's applicability by illustrating its workflow as Figure 6a and 6b.

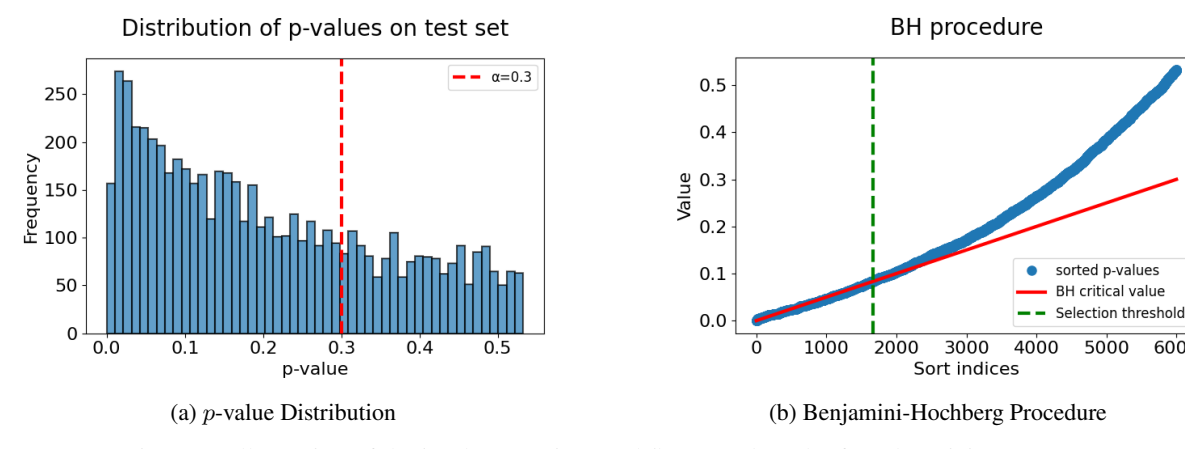


Figure 8: Illustration of the implementation workflow on *nlp* task of Real-Toxicity-Prompts.

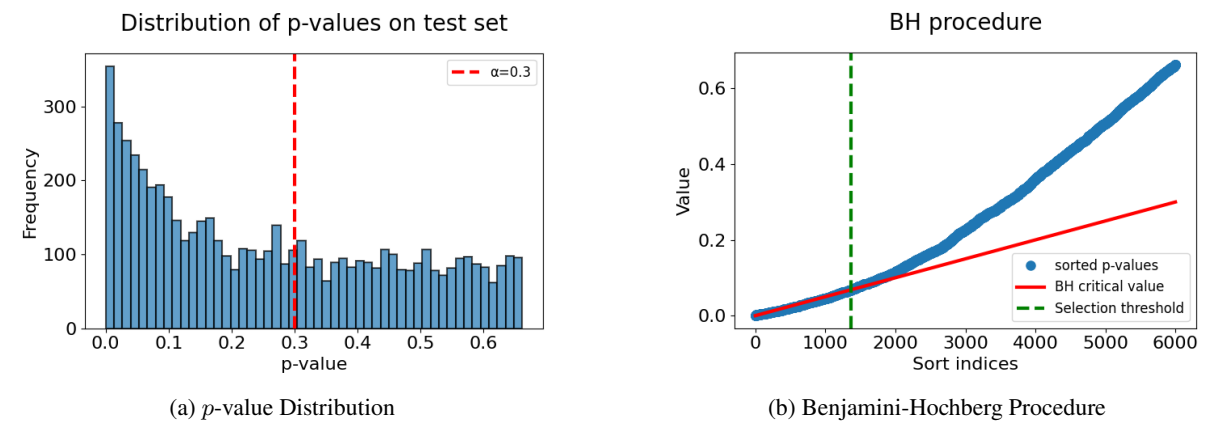


Figure 9: Illustration of the implementation workflow on *nlp* task of Pile-Toxicity-Balanced.

# C.3 Details of Tasks of vga

The VQA tasks are implemented through a pipeline that leverages conformal prediction to identify samples exhibiting high human annotation agreement within a predefined confidence interval. The method specifically targets an agreement score range from 0.28 to 0.82, designed to capture instances with moderate to strong annotator consensus. At the core of the system, the BLIP vision-language model is employed to generate answer predictions along with confidence scores. These scores are subsequently mapped to estimates of human agreement using two distinct regression techniques, Ridge and BayesianRidge regression, each providing a complementary approach to

modeling the relationship between model confidence and human consensus. The final selection of samples is performed using the *MCCS* (Multi-Class Calibrated Selection) method, which ensures rigorous control over the false discovery rate (FDR) throughout the inference process.

The VQA v2 dataset consists of 214,354 image-question pairs derived from the COCO 2014 validation set. Each question is associated with 10 human-annotated answers, facilitating the calculation of an agreement score, defined as the proportion of annotators who provided the most frequent response. This metric serves as a robust measure of consensus and label reliability. The implemented pipeline automatically downloads the COCO validation images, totaling 40,504, along with the corresponding questions and annotations. These components are processed through a customized VQA v2 Dataset class that systematically extracts and structures image-question-answer triplets, ensuring consistent and efficient data handling for subsequent modeling and analysis.

To ensure computational efficiency while preserving the essential statistical characteristics of the data, the implementation randomly samples a maximum of 1,000 image-question pairs. These samples are partitioned into training (80%), calibration (10%), and test (10%) subsets using random sampling, maintaining representative distributions across splits. The BLIP-VQA base model generates answer predictions along with confidence scores, obtained by averaging token probabilities during the text generation process. Meanwhile, human agreement scores are quantitatively defined as agreement =  $\frac{\text{count of the most frequent answer}}{10}$ , reflecting the consensus of annotators for each question. The implementation workflow for the vqa tasks is visually summarized in Figure 10, which follows the same structured format as Figure 6 to facilitate comparison and interpretation, thereby illustrating the method's practical applicability and scalability. Additionally, Figure 11 presents concrete examples of selected samples from the VQA tasks.

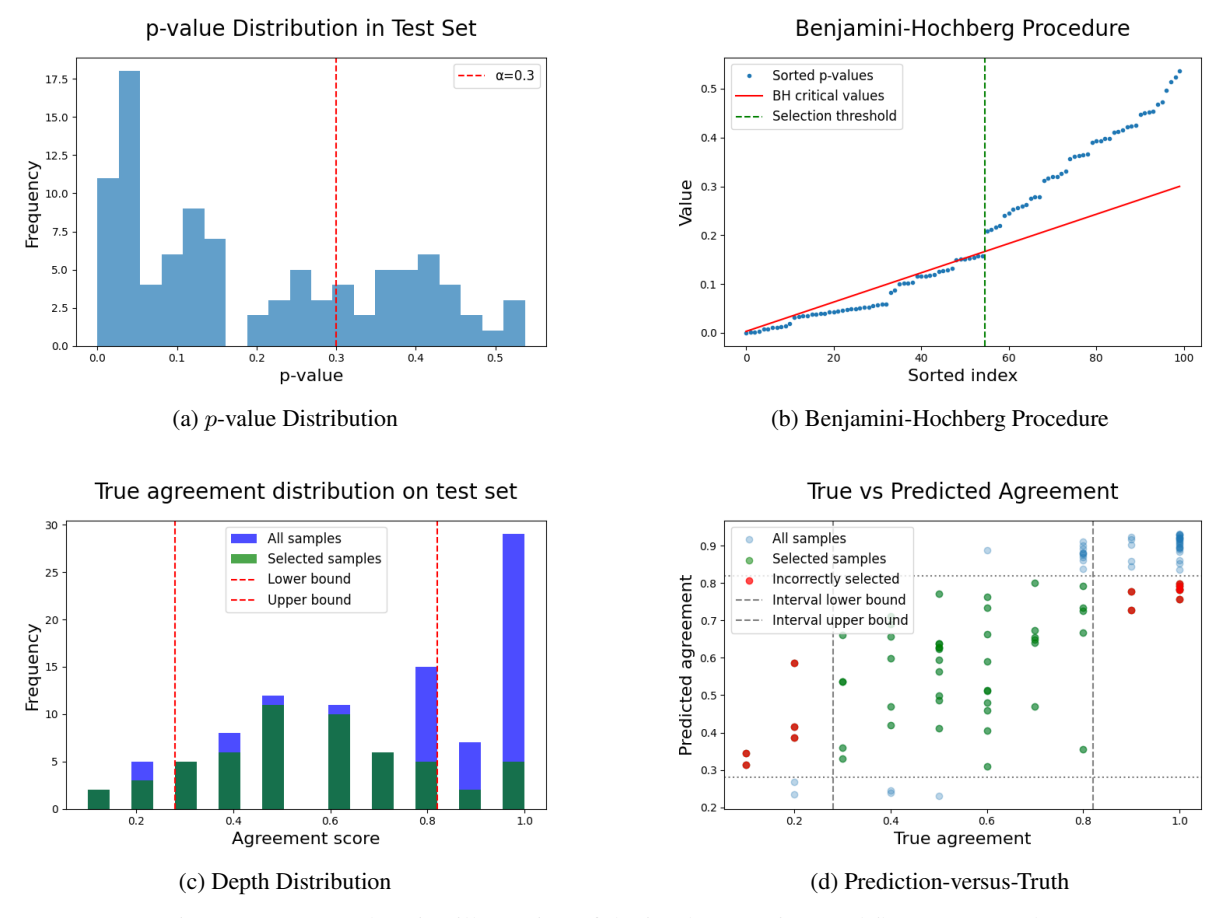


Figure 10: Comprehensive illustration of the implementation workflow on *vqa* tasks.

# Selected samples with moderately ambiguity

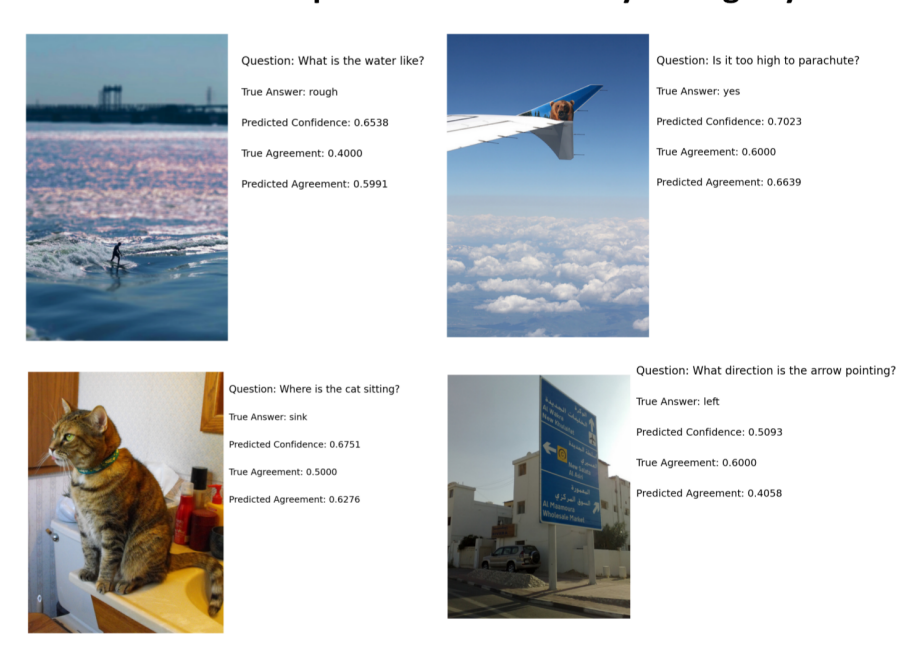


Figure 11: Selected Samples in the *vqa* Tasks.

# D Details of Multi-Class Tasks

### **D.1** Selection for Single-Class

The implementation of the *class* tasks on the CIFAR-10 dataset utilizes either ResNet or ViT architectures with FDR control in the *MCCS* approach to select specific images from multiple classes. The method accurately identifies target category samples (e.g., airplanes) while guaranteeing that the FDR remains below a predefined threshold, making it suitable for scenarios where only partial feature information of test samples is available. The core idea involves treating the multidimensional response not as a set of individually meaningful dimensions but rather as a holistic feature vector, thereby overcoming limitations inherent in existing approaches.

The CIFAR-10 dataset comprises  $60,000 \ 32 \times 32 \ RGB$  images across 10 classes: airplanes, automobiles, birds, cats, deer, dogs, frogs, horses, ships, and trucks, with 6,000 images per class, divided into 50,000 training and 10,000 test images. Data are partitioned via stratified sampling to preserve class balance: the test set contains 500 samples with equal representation of target/non-target classes, while the calibration set (also 500 samples) maintains 1:3 target-to-non-target ratio of CIFAR-10. The remaining samples comprise the training set, ensuring an adequate number of positive examples for prototype computation while maintaining realistic class distributions.

The class prototyping approach establishes discriminative decision boundaries within the fine-tuned feature space, drawing inspiration from ProtoNet by representing each class through an embedded prototype. The target class prototype  $\vec{p}$  is computed as the centroid of all target-class samples:  $\vec{p} = \frac{1}{n} \sum_{i=1}^{n} \vec{f_i}$ . A class-specific radius r, predefined according to the feature dimension, defines the acceptance region, with sample membership determined by the Euclidean distance metric  $\|\vec{f} - \vec{p}\|_2$ .

The regression component bridges the representational gap between feature domains via a MultiOutputRegressor with Ridge regression. This model learns a mapping:  $\mathbb{R}^{d_{\text{pretrained}}} \to \mathbb{R}^{d_{\text{fine-tuned}}}$  from pre-trained to fine-tuned feature spaces. Crucially, this mapping simulates the transformation from accessible features (e.g., pre-trained embeddings) to ideal but often unattainable features (e.g., fully fine-tuned representations), which can be substituted as needed in practical applications. Trained exclusively on the training partition, the regression model enables the inference-time prediction of task-adapted features from generic representations, enhancing applicability in real-world scenarios. By ensuring that the proportion of incorrectly selected samples remains below a predefined threshold (e.g., q = 0.1), this pipeline enables the reliable deployment of high-confidence predictions.

### **D.2** Selection for Multi-Class

The selection of multiple target classes, representing disjunctive conditions, naturally extends the application of *MCCS* in multi-class tasks. This approach facilitates the extension from single-class to multi-class selection via parallel hypothesis testing using class-specific prototypes. The proportion of target class samples in the calibration set is set to 0.65 to ensure adequate positive samples for prototype computation. Figure 12 illustrates sample selection outcomes using the target class of "airplanes" in the Single-Class Task and the target classes of "airplanes, automobiles, and birds" in the Multi-Class Task as examples.



Figure 12: Selected Samples in the Single-Class and Multi-Class Task.

## **D.3** Selection for Similar-Class

The selection of similar target classes, representing conjunctive conditions, naturally extends the application of *MCCS* in multi-class tasks as identifying samples within a specific distance threshold from a given class prototype. This experiment utilizes the CIFAR-100 dataset due to its inherent superclass structure, which provides ground-truth semantic groupings for evaluation. The proportion of target class samples in the calibration set was set to 0.5 to ensure balanced representation.

To summarize, the *MCCS* on multi-class tasks is validated using the CIFAR-10 [23] and CIFAR-100 [24] datasets, enabling the selection of individual (*class-A*), multiple (*class-B*), and similar (*class-C*) classes. Results at a nominal FDR level of 0.1 are presented in Table 10. Our method maintains rigorous FDR control across all the *class* tasks.

Figure 13 displays a selection of retrieved samples for the query class "dolphin" within the target superclass "aquatic mammals," and the class proportion within the selected samples. Notably, some incorrectly selected samples, such as "shark", which does not belong to the superclass yet exhibits visual similarity to dolphins, were also identified, illustrating the method's ability to capture perceptually coherent features despite occasional semantic mismatches, thereby underscoring the rationale behind the approach. Furthermore, the balanced selection across categories rather than focusing on a single class demonstrates the method's effectiveness in handling similarity, a property ensured by the circular region defined around class prototypes.

Table 10: Observed FDR and power for class Tasks at the nominal level 0.1.

Task	FDR	Power
class-A	0.084	0.994
class-B	0.094	0.733
class-C	0.096	0.643

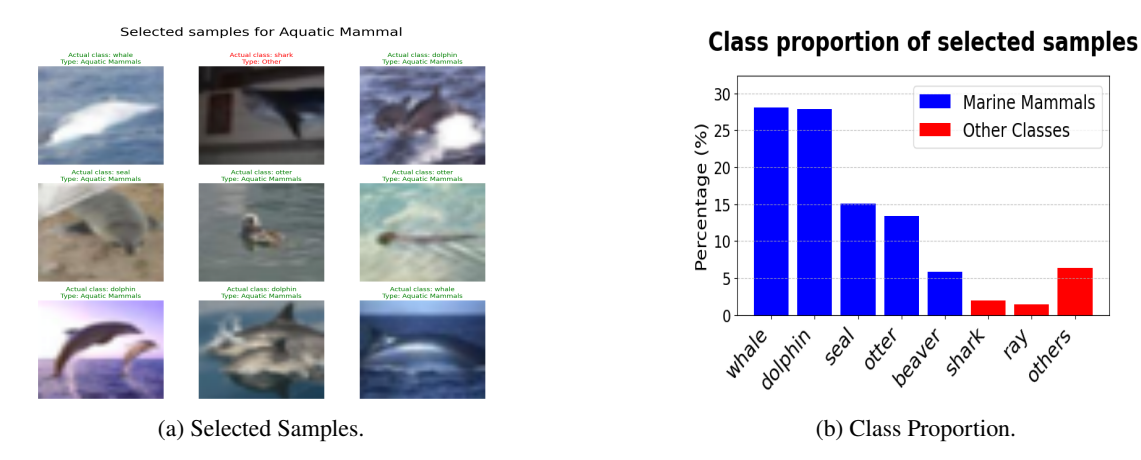


Figure 13: Selected Samples and Class Distribution in the Similar-Class Task.

# E Acknowledgment of The Use of Large Language Models (LLMs)

Large Language Models (LLMs) were used to aid in the writing and polishing of the manuscript. Specifically, we used an LLM to assist in refining the language, improving readability, and ensuring clarity in various sections of the paper. The model helped with tasks such as sentence rephrasing, grammar checking, and enhancing the overall flow of the text.

It is important to note that the LLM was not involved in the ideation, research methodology, or experimental design. All research concepts, ideas, and analyses were developed and conducted by the authors. The contributions of the LLM were solely focused on improving the linguistic quality of the paper, with no involvement in the scientific content or data analysis.

The authors take full responsibility for the content of the manuscript, including any text generated or polished by the LLM. We have ensured that the LLM-generated text adheres to ethical guidelines and does not contribute to plagiarism or scientific misconduct.